ORIGINAL RESEARCH PAPER
Pages: 51-64

FDFD Based Measurement of Permittivity Using an Open-ended Coaxial Probe

T. Shaterzadeh[1] and M. S. Majedi[2]
[1]*Computer and Communications Research Center, Ferdowsi University of Mashhad, Mashhad, Iran.*
[2]*Electrical Engineering Department, Ferdowsi university of Mashhad, Mashhad, Iran.*
majedi@um.ac.ir, t.shaterzade@gmail.com
Corresponding author: *majedi@um.ac.ir*

DOI: 10.22070/JCE.2022.15600.1206

***Abstract*- In this paper, 2D-FDFD method is applied for measuring electrical properties of dielectric materials using an open-ended coaxial probe. An SMA connector with flange is used as the coaxial probe and the reflection coefficient from probe aperture in contact with dielectric is measured by a vector network analyzer. To convert the aperture-plane reflection coefficient to dielectric permittivity, first, the coaxial probe is modeled by the 2D-FDFD method and then the genetic algorithm is employed to solve the inverse problem. The accuracy of the proposed method is investigated by measuring the dielectric properties of three known materials. The mean absolute percentage errors are below 10% and the maximum absolute percentage error is below 12%. A good agreement between measured and actual values are observed.**

***Index Terms*-** FDFD method, open-ended coaxial probe, permittivity.

I. INTRODUCTION

In general, the characterization of material properties at microwave frequencies has many application in various fields such as materials science, microwave system design, microwave absorber development, and biological research [1]. According to Table I, various methods have been proposed to determine the electromagnetic (EM) properties of materials [2]-[9]. Among them are methods based on open-ended coaxial probes. Broadband response, simplicity and the capacity for non-invasive measurements make these probes good candidate for electrical properties characterization [10]. Many researches have been published on using open-ended coaxial probe for EM properties measurement. These researches can be classified into two categories. The researches in the first category are based on simple models such as lumped element model (capacitive/radiation model) [2], virtual transmission line [4] and rational function model (RFM) [5],[6]. Although these models are simple and fast, they suffer from some limitations. For example, there are unknown frequency-independent variables in the equations of the lumped element model. To determine these unknown variables, materials with known electrical properties, which are called calibration materials, should.

Manuscript received 1-Sept.-2020 and revised 3-Dec.-2021, *P- ISSN: 2322-4088*
Accepted on 16- Feb.-2021 *E- ISSN: 2322-3936*

Table I. Brief comparison between various techniques for EM properteis measurements[2]-[9].

Measurement techniques	**Description**	**Mathematical Methods**	**Material properties**	**measured-parameters/ dielectric properties**
Transmission/ Reflection Line	Broadband (0.05-75 GHz), 2-port, destructive, 1 to 5% accuracy	Nicholson Ross -Weir (NRW)	Lossy solids, short, non-magnetics/magnetics	(S11, S21, S12, S22) or (S11, S21) / Mu, Epsilon
		NIST	Low loss solids, long, non-magnetics	(S11, S21, S12, S22) or (S11, S21) / Epsilon
		Poly Fit, Bartly	magnetics, not recommended for meta or left handed materials	(S11, S21, S12, S22) / Mu, Epsilon
		Short circuit line (SCL)	long samples for low loss materials	S11 / Epsilon
Open-ended coaxial probe	Broadband (0.2-50 GHz), 1-port, 1 to 10% accuracy, non-invasive	Lumped element model	Low loss materials	S11 / Epsilon
		Virtual transmission line	Lossy solids and liquids	
		Rational function model (RFM)	Applicable to an extensive range of materials (liquids, semi-solids, solids, powders...)	
		Analytical /semi-analytical full-wave analysis		
		Numerical simulations		
Free space	Broadband (5-500 GHz), 2-port, 1 to 2% accuracy, Need a flat surface	NRW	High temperature solids, large/ flat, non-magnetic	(S11, S21, S12, S22) or (S11, S21) / Mu, Epsilon
		NIST		(S11, S21, S12, S22) or (S11, S21) / Epsilon
Resonant Method (Cavity)	Single frequency (1-100 GHz), 0.1 to 2% accuracy, Destructive, need complicated algorithms	Frequency & Q-factors	Low loss solids, small, magnetic, non-magnetic	f, Q / Mu, Epsilon

be used. The sensitivity of the values of the unknown parameters to the calibration material properties can limit the accuracy of the measurement. Besides, the capacitive model is not suitable for high loss dielectric measurements and is valid at frequencies which the dimensions of the coaxial line are small compared to the wavelength [2], [11]. The results of experimental measurements have shown that the virtual transmission line model has an appropriate accuracy for measuring complex dielectric coefficients of materials such as biological tissues, however it has the same drawback of calibration

materials which explained above. In fact, the virtual transmission line model gives accurate results when the dielectric properties of calibration materials are close to those of the unknown material of under test. Experimental tests presented by [11] indicate that the RFM method gives good results while no calibration material is required. However, published RFM parameters are not completely suitable for different coaxial probes and hence a new set of parameters may be required to determine.

The second category of researches is based on analytical/semi-analytical full-wave analysis [12]-[15] and numerical simulations [16]-[21]. Although these methods are more difficult to implement, they have better accuracy. In the models of the first category and analytical/semi-analytical full-wave analysis methods, the material sample and coaxial probe flange dimensions are usually considered infinite. Using numerical methods such as FEM, FDTD and FDFD, the real geometry of the problem is considered and more precise results can be obtained. For example, FEM, FDTD and FDFD methods have been used to analyse the open-ended coaxial probe and to investigate the accuracy of other approaches [15]-[20]. In addition, the FDTD method has been used to determine the electromagnetic properties of concave surface materials [19],[20]. The FDFD method similar to FDTD has the capability of solving electromagnetics problems with complex geometries that are difficult to analyse by other methods [21]. In [21], it is indicated that the FDFD method is more efficient than FDTD method due to the short simulation time for analysing coaxial probe problems. Analysis of dispersive materials using frequency domain methods is easier compared to analysing them using time domain methods such as FDTD method [22]. In addition, discretization of Maxwell's equations can be implemented in a much simpler way than other frequency domain methods such as FEM [22].

In this paper, we present a new method based on using 2D-FDFD method along with the genetic algorithm to measure the dielectric properties of materials. In the next section, the theory of the proposed method is explained. To evaluate the accuracy of this method, the electrical properties of three materials are measured and the obtained results are compared with reference values in section III. Finally, we have the paper conclusion in the last section.

II. THEORY

To measure the dielectric properties of materials, first, a coaxial probe in contact with a dielectric material is connected to a vector network analyser (VNA) and the reflection coefficient of this probe at the aperture is measured. Then, according to the proposed method, the measured coefficient is converted to the permittivity coefficient. In this work, an SMA connector with flange, Fig. 1, is used as the coaxial probe and reflection coefficient of this probe at the aperture-plane is measured by the

Fig. 1. SMA connector used as a coaxial probe.

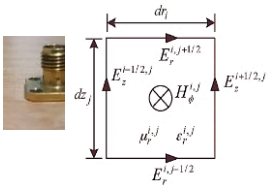

Fig.3. Two-dimensional finite difference cell in the cylindrical coordinates [21].

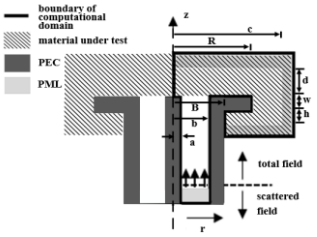

Fig. 2. Schematic of the finite flanged open-ended coaxial probe in contact with dielectric.

Agilent E8363B vector network analyser.

In the proposed method, the coaxial probe and the material under test are analysed using 2D-FDFD method. Therefore, the reflection coefficient of the probe aperture for materials with known permittivity can be computed by FDFD simulations. These simulations along with genetic algorithm optimization are used to determine the electrical properties of an unknown material from the reflection coefficient measured by VNA.

A. FDFD method for coaxial probe analysis

Fig. 2 shows the geometry of the problem. Due to the axial symmetry of the structure, the 2-D FDFD method is employed for the analysis of only one-half of the longitudinal cross-section. This leads to computational efficiency. The perfect matched layer (PML) boundary condition is used and the computational region is divided into the total field and the scattered field regions [21]. The incident wave source is considered at the total–scattered field region interface.

Due to the cylindrical symmetry of the geometry, we have $\partial/\partial\phi = 0$, and the modes which are excited at discontinuities are TM. The existing field components (E_r, E_z, H_ϕ) can be obtained by Maxwell equations as following

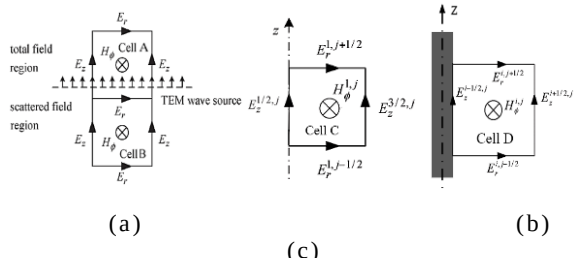

(a) (b) (c)

$$-\frac{\partial H_\phi}{\partial z} = j\omega\varepsilon_0\varepsilon_r PML_r E_r \tag{1}$$

$$\frac{1}{r}\frac{\partial}{\partial r}(rH_\phi) = j\omega\varepsilon_0\varepsilon_r PML_z E_z \tag{2}$$

$$\frac{\partial E_r}{\partial z} - \frac{\partial E_z}{\partial r} = -j\omega\mu_0\mu_r PML_\phi H_\phi \tag{3}$$

where

$$\begin{cases} PML_r = \dfrac{s_\phi s_z}{s_r} \\ PML_\phi = \dfrac{s_r s_z}{s_\phi} \\ PML_z = \dfrac{s_r s_\phi}{s_z} \end{cases} \tag{4}$$

and s_r , s_ϕ and s_z are the cylindrical coordinate stretching variables [23].

Maxwell's equations (1)-(3) are discretized using a two dimensional finite-difference cell of Fig. 3. Combining these discretized forms to eliminate the electric field components, the following equation is obtained [21]

$$A_1 H_\phi^{i-1,j} + A_2 H_\phi^{i+1,j} + A_3 H_\phi^{i,j-1} + A_4 H_\phi^{i,j+1} + A_5 H_\phi^{i,j} = 0 \tag{5}$$

Where

$$A_1 = \frac{-1}{dr_i}\frac{1}{r_{i-1/2}}\frac{1}{PML_z^{i-1/2,j}}\frac{2r_{i-1}}{\varepsilon_r^{i-1,j}dr_{i-1} + \varepsilon_r^{i,j}dr_i} \tag{5-a}$$

$$A_2 = \frac{-1}{dr_i}\frac{1}{r_{i+1/2}}\frac{1}{PML_z^{i+1/2,j}}\frac{2r_{i+1}}{\varepsilon_r^{i,j}dr_i + \varepsilon_r^{i+1,j}dr_{i+1}} \tag{5-b}$$

$$A_3 = \frac{-1}{dz_j}\frac{1}{PML_r^{i,j-1/2}}\frac{2}{\varepsilon_r^{i,j-1}dz_{j-1} + \varepsilon_r^{i,j}dz_j} \tag{5-c}$$

$$A_4 = \frac{-1}{dz_j}\frac{1}{PML_r^{i,j+1/2}}\frac{2}{\varepsilon_r^{i,j}dz_j + \varepsilon_r^{i,j+1}dz_{j+1}} \tag{5-d}$$

$$A_5 = -\left(\frac{r_i A_1}{r_{i-1}} + \frac{r_i A_2}{r_{i+1}} + A_3 + A_4 + \omega^2\varepsilon_0\mu_0\mu_r^{i,j}PML_\phi^{i,j}\right) \tag{5-e}$$

and r_i is the distance between the centre of the cell and the axis of the probe.

According to Fig. 4(a), the incident TEM wave source is applied on the total-scattered field boundary. The EM field components of the incident wave are as follows [21]

$$E_{rinc}^{i,j+1/2} = \frac{U_{inc}}{\ln(b/a)} \frac{1}{r_i + a} \exp\left[-j\omega\sqrt{\mu_c \varepsilon_c}(z_j + 0.5dz_j) \right] \tag{6}$$

$$H_{\phi inc}^{i,j} = \sqrt{\varepsilon_c / \mu_c} \frac{U_{inc}}{\ln(b/a)} \frac{1}{r_i + a} \exp(-j\omega\sqrt{\mu_c \varepsilon_c} z_j) \tag{7}$$

where z_j, a, b, μ_c and ε_c are the distance between the centre of the cell and the input of the probe, the inner and outer radius of the coaxial probe, and the complex permeability and permittivity of the coaxial dielectric, respectively.

The cells in the computational region are classified into five types. The cells that the total–scattered field region interface crosses (cell A in Fig. 4(a)), the cells just below the total–scattered field region interface (cell B in Fig. 4(a)), the cells next to the z-axis (cell C in Fig. 4(b)), the cells next to the PEC (cell D in Fig. 4(c)) and other cells.

It can be shown that cells in the first and second category are described by the following equations, respectively [21]

$$A_1 H_\phi^{i-1,j} + \ldots + A_5 H_\phi^{i,j+1} = \frac{1}{dz_j} \frac{1}{PML_r^{i,j-1/2}} \times \frac{2H_{\phi inc}^{i,j}}{\varepsilon_r^{i,j-1} dz_{j-1} + \varepsilon_r^{i,j} dz_j} + \frac{1}{dz_j} j\omega\varepsilon_0 E_{rinc}^{i,j-1/2} \tag{8}$$

$$A_1 H_\phi^{i-1,j} + \ldots + A_5 H_\phi^{i,j} = \frac{1}{dz_j} \frac{1}{PML_r^{i,j+1/2}} \times \frac{-2H_{\phi inc}^{i,j+1}}{\varepsilon_r^{i,j} dz_j + \varepsilon_r^{i,j+1} dz_{j+1}} \tag{9}$$

For the third category, Equation (5) can be used with A_1 and A_5 replacing by [21]

$$\begin{cases} A_1 = 0 \\ A_5 = -\left(\frac{r_1 A_2}{r_2} + A_3 + A_4\right) + \left(\omega^2 \varepsilon_0 \mu_0 \mu_r^{1,j} PML_\phi^{1,j} + \left(\frac{1}{dr_i}\right)^2 \frac{4}{\varepsilon_r^{1,j} PML_z^{1/2,j}}\right) \end{cases} \tag{10}$$

For the cells next to the PEC, the electric field component on the surface of the PEC is zero. For example, if the index of cell D in Fig. 4(c) is (i, j), the electric field component $E_z^{i-1/2,j}$ in the discretized form of (2) should be set to zero. Thus, it can be shown that cell D is described by (5) with A_1=0. In general, for cells in which one of the electric field components ($E_z^{i-1/2,j}$, $E_z^{i+1/2,j}$, $E_r^{i,j-1/2}$, $E_r^{i,j+1/2}$) is zero, the coefficients in (5) should be revised as following

$$\begin{cases} E_z^{i-1/2,j} = 0: \ \mathrm{A}_1 = 0 \\ E_z^{i+1/2,j} = 0: \ \mathrm{A}_2 = 0 \\ E_r^{i,j-1/2} = 0: \ \mathrm{A}_3 = 0 \\ E_r^{i,j+1/2} = 0: \ \mathrm{A}_4 = 0 \end{cases} \tag{11}$$

Finally, Equation (5) is used for other cells.

In summary, a linear set of equations can be obtained as follows

$$[A][X]=[F] \tag{12}$$

where [*A*] is the coefficients matrix, [*X*] is the unknown matrix of the variables H_ϕ, and [*F*] is related to TEM wave source. Determining H_ϕ components by solving equation (13), *E* components can be obtained from the discretized form of (1) and (2). According to the reference plane at the interface between cell A and B in Fig. 4(a), the reflection coefficient of TEM mode can be calculated as follows [21]

$$\Gamma = \frac{V_{ref}^{j+1/2}}{V_{inc}^{j+1/2}} \tag{13}$$

where V_{ref} and V_{inc} are the reflected and the incident voltages, respectively, and are be obtained as follows [21]

$$V_{ref}^{j+1/2} = \int_a^b E_r^{j+1/2} dr \approx \sum_i E_r^{i,j+1/2} dr_i \tag{14}$$

$$V_{inc}^{j+1/2} = \int_a^b E_{rinc}^{j+1/2} dr \approx \sum_i E_{rinc}^{i,j+1/2} dr_i \tag{15}$$

The E_r components in (15) are obtained from the discretized form of (1) for the cells just below the total–scattered field region interface as follows [21]

$$E_r^{i,j+1/2} = \frac{1}{j\omega\varepsilon_0} \frac{2}{\varepsilon_r^{i,j} dz_j + \varepsilon_r^{i,j+1} dz_{j+1}} \times \frac{1}{PML_r^{i,j+1/2}} \left[H_\phi^{i,j} - (H_\phi^{i,j+1} - H_{\phi inc}^{i,j+1}) \right] \tag{16}$$

The reflection coefficient at the probe aperture can be calculated by de-embedding Γ as follows

$$\Gamma_a = \Gamma \exp(2j\beta_0 d) \tag{17}$$

where β_0 is the propagation constant of the coaxial probe and *d* is the distance between the original reference plane and the probe aperture.

B. Electrical properties calculation

In this section, the genetic algorithm as an optimization tool is employed to compute the relative

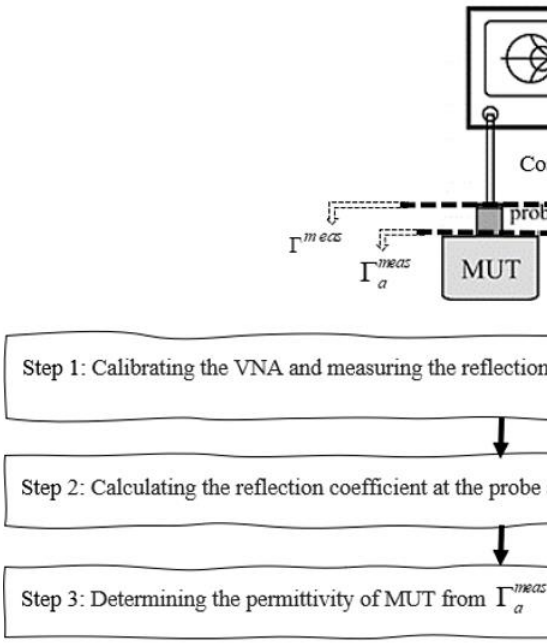

Fig. 5. Calibration process and permitivity calculation procedure.

complex permittivity ($\varepsilon_r = \varepsilon_r' - j\,\varepsilon_r'' = \varepsilon_r' - j\,\sigma/\omega\varepsilon_0$) from the reflection coefficient measured by VNA.

The goal of an optimization process is to minimize a given objective function value under a specific set of constraints. In the genetic algorithm, first, an initial population of solutions (called chromosomes) is generated. Each solution is evaluated by the objective function and the best solutions (chromosomes) are selected and modified using operators such as recombination (crossover) and mutation, to form a new population. In the next iteration, a portion of the best solutions of the previous and new population are selected to form a new generation. The algorithm terminates when either a maximum number of generations is produced, or the objective function value reaches the specified value.

In this problem, the objective function of the GA is defined as

$$\text{Objective Function}=\left[real(\Gamma_a^{meas}-\Gamma_a^{FDFD})\right]^2+\left[imag(\Gamma_a^{meas}-\Gamma_a^{FDFD})\right]^2 \tag{18}$$

where G_a^{meas} and G_a^{FDFD} are measured reflection coefficient by VNA and the calculated one by the FDFD simulation, respectively.

The VNA reference plane for the reflection coefficient measurement is at the entrance of the probe. Note that de-embedding the coaxial cable between VNA and SMA is done by the use of calibration kit including open, short, and load. To determine the desired reflection coefficient at the probe aperture, we consider the probe as a two-port microwave network, in which *S*-parameters relate the reflection coefficient measured by VNA (G^{meas}) to the reflection coefficient at the aperture plane (G_a^{meas}) as follows [10]

Fig. 6. Generated chromosomes

Fig. 7.

$$\Gamma^{meas} = S_{11} + \frac{S_{12}S_{21}\Gamma_a^{meas}}{1 - S_{22}\Gamma_a^{meas}} \tag{19}$$

To determine the three combinations of S-parameters, S_{11}, S_{22}, and $S_{12}S_{21}$ in (19), we use three reference materials (air, distilled water, and methanol) along with measured data for Γ^{meas} and simulated data, obtained by FDFD method, for Γ_a^{meas}. Fig. 5 shows the calibration process and permittivity calculation procedure.

In the optimization procedure, the relative complex permittivity is defined in terms of four variables, according to (20). In fact, a set of four integers in the range (0-100) is generated as a chromosome (Fig.6). Assuming the real and imaginary part of the relative permittivity are decimal numbers in the range 0 to 100, the first and third numbers of chromosomes are considered as the integer part and, the second and fourth numbers are considered for the decimal part. In most cases we know the approximate range of the dielectric coefficients in bandwidth, so the solution search domain in GA code can be defined smaller and more precisely.

$$\varepsilon = e_1 + \frac{e_2}{100} - (e_3 + \frac{e_4}{100})\, j \tag{20}$$

III. NUMERICAL RESULTS

To evaluate the accuracy of the proposed method, the complex permittivity of the Saline 0.5 M as a high loss liquid medium with high dielectric constant, ethanol with low electrical properties, and Teflon as a solid material with a low dielectric constant are measured in the range of 0.1-18 GHz. The setup for measuring the reflection coefficients of the materials is shown in Fig. 7. The liquids volume is about 250 ml and the distance of the probe from the bottom of the beaker is more than 30 mm. The radius and height of the solid sample (Teflon) is 20 mm and 40 mm, respectively.

Computational domain is discretized with a mesh size of 0.1 mm and the PML length is set to 1 mm. In the simulation code, the dimensional parameters of the coaxial probe and the dielectric material, as indicated in Fig. 2, are $2a$ = 1.3 mm, $2b$ = 4.1 mm, R = 5 mm, B = 2.1 mm, c = 7 mm, d = 2 mm, w =1 mm, h = 1 mm.

The 2D-FDFD method and the genetic algorithm are implemented in MATLAB 2019 on a personal computer with core i7-32 GB RAM. The simulation time of the FDFD algorithm for each frequency is about 2.3s. In the GA code, the number of population and iterations (termination condition) are considered 50 and 40, respectively. At a certain frequency point, the run time of optimization to find the relative permittivity is about 75 min. Fig. 8 shows the comparison between the dielectric constant and conductivity measured by the proposed method and the theoretical ones for Saline 0.5 M, ethanol and Teflon [24]-[26].

Table II summarizes the Cole-Cole parameters reported by [24],[25] for saline solution, ethanol and calibration materials (distilled water and methanol). The Cole-Cole equation is given as [24]

$$\varepsilon = \varepsilon^{'} - j\varepsilon^{''} = \varepsilon_{\infty} + \frac{\varepsilon_s - \varepsilon_{\infty}}{1+(j\omega\tau)^{1-\alpha}} - j\frac{\sigma_i}{\varepsilon_0\omega} \tag{21}$$

where ε_{∞} is the optical permittivity, ε_s is the static permittivity, τ is the relaxation time, α is the distribution parameter and σ_i is the ionic conductivity of the liquids.

Table II. Cole-Cole parameters of references and test liquids [24, 25].

Material	ε_s	ε_{∞}	$\tau(ps)$	α	σ_i
distilled water	78.5	5.2	8.3	0	0
methanol	33	5.33	53.29	0	0
Saline 0.5 M	69.257	4.9	7.995	0	4.68
ethanol	25.4	4.38	177.23	0	0

Table III. Mean Absolute Percentage error of electrical properties of test materials

	Saline 0.5 M	**Ethanol**	**Teflon**
MAPE (%)	4.6	5.72	9.21

In Fig. 8, the curves show good agreement between measured and reference data. Table III reports the magnitude of mean absolute percentage error (MAPE) for electrical properties of the Saline solution, ethanol and Teflon, computed as follows

$$MAPE = \frac{100}{N}\sum_{N}\left|\frac{\varepsilon_{ref} - \varepsilon_{meas}}{\varepsilon_{ref}}\right| \tag{22}$$

where ε_{ref} and $\varepsilon_{\text{meas}}$ are the reference relative permittivity and measured ones, respectively, and N is the number of frequency points.

From Table III, it can be seen that the MAPE values are below 10%. The maximum absolute percentage error at the frequency range of 6-12 GHz, which is a common range for many applications, is 4.3% (saline), 11.4% (ethanol) and 11.8% (Teflon). This accuracy can be acceptable as the maximum

error is below 12% and the MAPE values in this rang are respectively 3% (saline), 3.3% (ethanol) and 11.21% (Teflon).

The errors of the results may be due to following factors

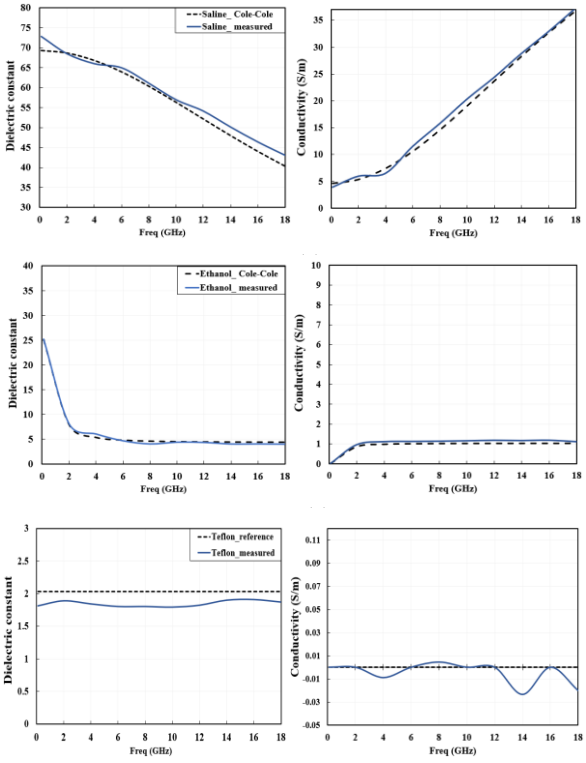

(e)
(f)

Table IV. Comparision of proposed method and other open-ended coaxial probe based methods

Methods	Speed	Dependency on calibration materials	Closed form relation	Accuracy	Complexity
Lumped element	High	YES	YES	Low	Low
Virtual transmission Line	High	YES	YES	Medium	Low
RFM	High	NO	YES	Medium	Medium
Analytical/ semi-analytical full-wave analysis	Medium	NO	NO	Medium	Medium
Proposed method	Low	NO	NO	High	High

- Systematic errors which have not been completely eliminated along with random errors have affected the accuracy of reflection measurement. In the case of Teflon as a solid, some of the error is due to that the probe was not completely in contact with the sample and there was an air gap between the probe and Teflon.
- The numerical calculation of reflection coefficient by the FDFD method has some errors.
- The purity of the materials used in this study, such as ethanol and saline, was not exactly the same as that of materials used for Cole-Cole parameter extraction.

Table IV, compares the proposed method with other open-ended coaxial probe based methods.

IV. CONCLUSION

In this paper, a new method based on 2D-FDFD along with the genetic algorithm is proposed to determine the complex permittivity of solid and liquid materials by an open-ended coaxial probe. According to this method, 2D-FDFD is applied to analyse the coaxial probe and the material under test with known parameters. On the other hand, the GA, as an optimization algorithm, is used to solve the inverse problem based on the measured values by VNA and simulated values by 2D-FDFD.

Validation studies conducted using three known materials, i.e., saline 0.5 M, ethanol, and Teflon in the frequency range of 0.1-18 GHz. MAPE values in these measurements are below 10% and hence there is an acceptable agreement between the theoretical values and experimental results obtained in this paper. Therefore, the proposed method can be a good choice for electrical measurements of unknown materials in a broadband frequency range of 0.1-18 GHz.

REFERENCES

[1] L.-F. Chen, C. Ong, C. Neo, V. Varadan, and V. K. Varadan, *Microwave electronics: measurement and materials characterization*. John Wiley & Sons, 2004.

[2] T. W. Athey, M. A. Stuchly, and S. S. Stuchly, "Measurement of radio frequency permittivity of biological tissues with an open-ended coaxial line: Part I," *IEEE Tran. Microwave Theory Techniques,* vol. 30, no. 1, pp. 82-86, Jan. 1982.

[3] M. D. Janezic and J. A. Jargon, "Complex permittivity determination from propagation constant measurements," *IEEE Microwave And Guided Wave Letters,* vol. 9, no. 2, pp. 76-78, Feb. 1999.

[4] F. M. Ghannouchi and R. G. Bosisio, "Measurement of microwave permittivity using a six-port reflectometer with an open-ended coaxial line," *IEEE Trans. Instrumentation and Measurement,* vol. 38, no. 2, pp. 505-508, April 1989.

[5] S. Stuchly, C. Sibbald, and J. Anderson, "A new aperture admittance model for open-ended waveguides," *IEEE Trans. Microwave Theory And Techniques,* vol. 42, no. 2, pp. 192-198, Feb. 1994.

[6] J. Anderson, C. Sibbald, and S. Stuchly, "Dielectric measurements using a rational function model," *IEEE Trans. Microwave Theory Techniques,* vol. 42, no. 2, pp. 199-204, Feb. 1994.

[7] K. C. Yaw, *Measurement of dielectric material properties* (Application Note. Rohde & Schwarz). April 2012, pp. 1-35.

[8] M. D. Pérez Cesaretti, "General effective medium model for the complex permittivity extraction with an open-ended coaxial probe in presence of a multilayer material under test," Ph.D. dissertation, Uppsala University, Bologna, Italy, May 2012.

[9] Keysight, "Automate Complex Permittivity and Permeability Measurements with Keysight's Materials Measurement Software Suite," in "N1500A Materials Measurement Suite technical overview. Keysight technologies," January 2021. [Online]. Available: www.keysight.com

[10] D. Popovic *et al.*, "Precision open-ended coaxial probes for in vivo and ex vivo dielectric spectroscopy of biological tissues at microwave frequencies," *IEEE Trans. Microwave Theory Techniques,* vol. 53, no. 5, pp. 1713-1722, May 2005.

[11] D. Berube, F. Ghannouchi, and P. Savard, "A comparative study of four open-ended coaxial probe models for permittivity measurements of lossy dielectric/biological materials at microwave frequencies," *IEEE Trans. Microwave Theory Techniques,* vol. 44, no. 10, pp. 1928-1934, May 1996.

[12] D. V. Blackham and R. D. Pollard, "An improved technique for permittivity measurements using a coaxial probe," *IEEE Trans. Instrumentation Measurement,* vol. 46, no. 5, pp. 1093-1099, Oct. 1997.

[13] P. De Langhe, K. Blomme, L. Martens, and D. De Zutter, "Measurement of low-permittivity materials based on a spectral-domain analysis for the open-ended coaxial probe," *IEEE Trans. Instrumentation Measurement,* vol. 42, no. 5, pp. 879-886, Oct. 1993.

[14] C.-L. Li and K.-M. Chen, "Determination of electromagnetic properties of materials using flanged open-ended coaxial probe-full-wave analysis," *IEEE Trans. Instrumentation Measurement,* vol. 44, no. 1, pp. 19-27, Feb. 1995.

[15] R. Olmi, M. Bini, R. Nesti, G. Pelosi, and C. Riminesi, "Improvement of the permittivity measurement by a 3D full-wave analysis of a finite flanged coaxial probe," *Journal of Electromagnetic Waves Applications,* vol. 18, no. 2, pp. 217-232, April 2004.

[16] P. De Langhe, L. Martens, and D. De Zutter, "Design rules for an experimental setup using an open-ended coaxial probe based on theoretical modelling," *IEEE Trans. Instrumentation Measurement,* vol. 43, no. 6, pp. 810-817, Dec. 1994.

[17] G. B. Gajda and S. S. Stuchly, "Numerical analysis of open-ended coaxial lines," *IEEE Trans. Microwave Theory Techniques,* vol. 31, no. 5, pp. 380-384, May 1983.

[18] D. M. Hagl, D. Popovic, S. C. Hagness, J. H. Booske, and M. Okoniewski, "Sensing volume of open-ended coaxial probes for dielectric characterization of breast tissue at microwave frequencies," *IEEE Trans. Microwave Theory Techniques* vol. 51, no. 4, pp. 1194-1206, April 2003.

[19] A. K. A. Hassan, D. Xu, N. Maode, and Y. J. Zhang, "EM properties measurement of concave surface coating materials using a modified open ended coaxial probe," *Microwave Optical Technology Letters*, vol. 27, no. 4, pp. 278-281, Sept. 2000.

[20] A. K. A. Hassan, D. Xu, and Y. Zhang, "Modeling and analysis of finite flange open ended coaxial probe for planar and convex surface coating material testing by FDTD method," *Microwave Optical Technology Letters,* vol. 24, no. 2, pp. 117-120, Dec. 2000.

[21] R. Huang and D. Zhang, "Analysis of open-ended coaxial probes by using a two-dimensional finite-difference frequency-domain method," *IEEE Trans. Instrumentation Measurement,* vol. 57, no. 5, pp. 931-939, May 2008.

[22] W. Shin, "3D finite-difference frequency-domain method for plasmonics and nanophotonics," Ph.D. dissertation, Stanford University, California, United States, Aug. 2013.

[23] W. C. Chew, J. Jin, and E. Michielssen, "Complex coordinate stretching as a generalized absorbing boundary condition," *Microwave and Optical Technology Letters,* vol. 15, no. 6, pp. 363-369, Dec. 1997.

[24] A. Nyshadham, C. L. Sibbald, and S. S. Stuchly, "Permittivity measurements using open-ended sensors and reference liquid calibration-an uncertainty analysis," *IEEE Trans. Microwave Theory and Techniques,* vol. 40, no. 2, pp. 305-314, Feb. 1992.

[25] E. Piuzzi *et al.*, "A comparative analysis between customized and commercial systems for complex permittivity measurements on liquid samples at microwave frequencies," *IEEE Trans. Instrumentation and Measurement,* vol. 62, no. 5, pp. 1034-1046, May 2013.

[26] W. B. Weir, "Automatic measurement of complex dielectric constant and permeability at microwave frequencies," *Proceedings of the IEEE,* vol. 62, no. 1, pp. 33-36, Jan. 1974.